Local Spectral Analysis of Short-Pulse Excited Scattering from Weakly Inhomogeneous Media—Part I: Forward Scattering

Timor Melamed, Ehud Heyman, *Senior Member, IEEE*, and Leopold B. Felsen, *Life Fellow, IEEE*

***Abstract*— In this two-part sequence, we extend a previously formulated pulsed plane wave (PPW)-based time-domain (TD) diffraction tomography [1] for forward and inverse scattering from weakly inhomogeneous lossless nondispersive media to a more highly localized pulsed beam (PB) wavepacket-based diffraction tomography. In the PPW version, the incident and scattered fields have been parameterized in the space-time wavenumber domain in terms of slant-stacked TD plane waves whose wavefronts move through the scattering medium at the ambient propagation speed, thereby accumulating information along time-resolved laterally extended planar cuts. The PB parameterized localization confines the laterally sampled regions to the spatial domains of influence transverse to the relevant beam axes. These localizations are performed in two stages. The present paper implements the PB parameterization by PB post processing of the forward scattered fields excited by an incident PPW; the companion paper [2] deals with the inverse problem by back propagation of the PB parameterized data. An "ultimate" localization of a space-time resolved scattering cell, achieved via scattered and incident PB's (PB post and preprocessing) will be addressed elsewhere, but is briefly summarized in [2].**

***Index Terms*— Electromagnetic scattering, inverse problems, nonhomogeneous media, pulsed beams.**

I. Introduction

As stated in the abstract, the present two-part study is concerned with extending the previously formulated pulsed plane wave (PPW)-based global (along entire plane cuts) time-domain (TD) diffraction tomography for forward and inverse scattering in [1] and [3] to a highly localized transversely confined pulsed-beam (PB) wavepacket-based tomography. Due to space limitations, we cannot present the step-by-step evolution of the local PB from the global PPW formulation; instead, we address both formulations directly. Accordingly, the presentation here is confined to the new material and it is assumed that *the reader is familiar with references* [1], [4], which are extensively cited in what follows: [1] addresses the inverse problem using the global (PPW) approach while [4] presents an extensive analytical and numerical study of the local (PB) processing tools, which will be utilized here in connection with the inverse problem.

After stating the problem in Section II, we define in Section III the various spectral forward and inverse global (nonwindowed) and local (windowed) transforms and introduce phase-space terminology. Windowed transforms are treated in detail in Section III-B2 as the PB-parameterized extensions of the previous PPW algorithms and the physical properties in the phase space of the corresponding PB propagators are summarized in Section III-B3 [4]. After these preliminaries, the previous PPW-based weak (Born) scattering formalism [1] is generalized in Section IV to its PB-based windowed extension. The general formulation is presented in Section IV-B and then interpreted phenomenologically in Section IV-B. Noteworthy is the PB generalized version of the PPW "pseudoreflection rule" in [1] pertaining to the scattering process, which turns out to be explained more naturally in terms of point-to-point PB-constrained ray paths instead of the global PPW wavefronts. The phase-space formalism is demonstrated for two classes of window functions (processing algorithms): A PPW window (Section IV-D) that produces the same results as in [1] and a Gaussian δ window (Section IV-E), which yields analytically tractable PB propagators of the type developed in [5]–[7]. In [2], these propagators will be used to backpropagate the field and to produce the local inverse. Conclusions are summarized in Section V.

II. Statement of the Problem

Via interrogation by a time-dependent scalar plane wave field $u^i(\mathbf{r}, t)$, we consider the scattering by, and reconstruction of, an inhomogeneous nondispersive lossless medium of compact support, characterized by a wave speed $v(\mathbf{r})$ (which is to be *determined* in the inverse problem) and embedded in a uniform background with wave speed v_o. Throughout, $\mathbf{r}$ is a position vector in a three-dimensional (3-D) coordinate space with bold face types identifying vector quantities. The total field $u(\mathbf{r}, t)$ satisfies the wave equation

$$\left[\nabla^2 - \frac{1}{v^2(\mathbf{r})}\,\partial_t^2\right] u(\mathbf{r},t) = 0, \qquad \partial_t \equiv \partial/\partial t \tag{1}$$

Manuscript received September 3, 1997; revised January 5, 1998. This work was supported in part by the U.S.–Israel Binational Science Foundation, Jerusalem, Israel, under Grants 92-00273 and 95-00399, the 1996–1997 Dean's Postdoctoral Fellowship, Boston University, the U.S. Air Force Office of Scientific Research under Grant 96-1-0039, and the Naval Coastal Systems Center, Panama City, FL, under ONR Grant N61331-96-K-0028.

T. Melamed and E. Heyman are with the Department of Electrical Engineering, Physical Electronics, Tel-Aviv University, Tel-Aviv, 69978 Israel.

L. B. Felsen is with the Department of Aerospace and Mechanical Engineering and the Department of Electrical and Computer Engineering, Boston University, Boston, MA 02215 USA.

Publisher Item Identifier S 0018-926X(99)05817-2.

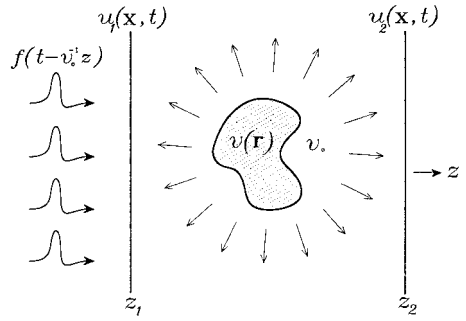

Fig. 1. Physical configuration. The object function $O(\mathbf{r})$ is illuminated by a transient plane wave $f(t-v_o^{-1}z)$ propagating along the z axis. The scattered field $u_j(\mathbf{x}, t)$ is measured on the planes $z = z_j$, $j = 1, 2$ between which the object is situated.

and, for convenience, the unknown medium is described by the *object function*

$$O(\mathbf{r}) = [v_o/v(\mathbf{r})]^2 - 1. \tag{2}$$

The compact object domain is assumed to be located between two measurements planes at z_1 and z_2 whereon the scattered field is measured (Fig. 1). The incident time-dependent wave field is

$$u^i(\mathbf{r}, t) = f\Big(t - v_o^{-1}\mathring{\boldsymbol{\kappa}}^i \cdot \mathbf{r}\Big) \tag{3}$$

where $f(t)$ specifies the pulse shape and $\mathring{\boldsymbol{\kappa}}^i$ is a unit vector in the propagation direction (henceforth, the symbol $\circ$ identifies a unit vector). Coordinates are chosen so that the incident field propagates along the z direction, i.e., $\mathring{\boldsymbol{\kappa}}^i \equiv \mathring{\mathbf{z}}$. The space coordinate points are, therefore, labeled $\mathbf{r} = (\mathbf{x}, z)$ with $\mathbf{x} = (x_1, x_2)$ and the data (the scattered field) at the $z_{1,2}$ planes is denoted, respectively, by $u_{1,2}(\mathbf{x}, t)$. We shall use the index $j = 1, 2$ to tag quantities pertaining to data on the z_j planes, respectively.

III. Spectral Analysis and Synthesis: Operations

In this section, we summarize the phase-space analysis and synthesis formalisms that parameterize the fields on the observation planes z_j, $j = 1, 2$ and transport them from these planes into the unperturbed environment.

A. Time-Frequency Relations

Our TD and frequency-domain (FD) constituents are related via

$$u(t) = \frac{1}{2\pi}\int_{-\infty}^{\infty} \hat{u}(\omega)e^{-i\omega t}\, d\omega \tag{4}$$

where the caret $\hat{}$ denotes time-harmonic field constituents throughout.

In certain cases it will be convenient to use the analytic signal counterpart, to be denoted by the symbol $^+$ and defined by the one-sided Fourier inversion

$$\overset{+}{u}(t) = \frac{1}{\pi}\int_0^{\infty} d\omega e^{-i\omega t}\hat{u}(\omega), \qquad \mathrm{Im}t \le 0. \tag{5}$$

This integral representation can accommodate complex t with $\mathrm{Im}t \le 0$; the limit for real t is related to the real signal $u(t)$ via $\overset{+}{u}(t) = u(t) + i\mathcal{H}_t u(t)$, where $\mathcal{H}_t = (\mathcal{P}/\pi t)\overset{t}{\otimes}$ is the Hilbert transform operator with $\mathcal{P}$ denoting Cauchy's principal value and $\overset{t}{\otimes}$ denoting a convolution. The real field for real t is, therefore, obtained via $u(t) = \mathrm{Re}\overset{+}{u}(t)$. The analytic signal representation has been used extensively for TD wave propagation and scattering problems, in particular those that involve evanescent spectra identified by complex time delay (e.g., [4]–[6], [8], [9]).

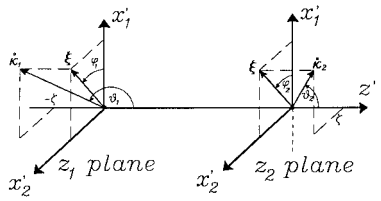

Fig. 2. Plane wave scattering directions. Scattering takes place along the negative z axis with respect to z_1 and along the positive z axis with respect to z_2, with corresponding scattering directions defined by $\mathring{\boldsymbol{\kappa}}_j = (\boldsymbol{\xi}, \mp\zeta)$.

B. Space-Wavenumber Relations

1) Nonwindowed (Global) Transforms: Conventional plane wave spectral analysis and synthesis of the time-harmonic fields $\hat{u}_j(\mathbf{x}, \omega)$ is performed via the global Fourier transforms

$$\hat{\tilde{u}}_j(\boldsymbol{\xi}) = \int_{-\infty}^{\infty} d^2x \hat{u}_j(\mathbf{x})e^{-ik\boldsymbol{\xi}\cdot\mathbf{x}}, \quad \boldsymbol{\xi} = (\xi_1, \xi_2), \quad k = \omega/v_o \tag{6a}$$

$$\hat{u}_j(\mathbf{x}) = \left(\frac{k}{2\pi}\right)^2 \int_{-\infty}^{\infty} d^2\xi \hat{\tilde{u}}_j(\boldsymbol{\xi})e^{ik\boldsymbol{\xi}\cdot\mathbf{x}} \tag{6b}$$

where $\tilde{}$ identifies a wavenumber spectrum function. The dimensionality of the integration is identified by that of the differential d^2x; infinite integration limits $\pm\infty$ will be understood and omitted in the notation. Anticipating extension to the TD, the vector spatial wavenumber $\boldsymbol{\xi}$ has been normalized with respect to the ambient medium wavenumber $k = \omega/v_o$ so that $\boldsymbol{\xi}$ has a frequency-independent direct geometrical interpretation in terms of the spectral plane wave propagation angles. Specifically, $\hat{\tilde{u}}_j(\boldsymbol{\xi})$ describes the scattered spectral plane wave arriving at the z_j plane along the unit vector direction

$$\begin{aligned}\mathring{\boldsymbol{\kappa}}_j &= (\boldsymbol{\xi}, \mp\zeta)\\ &= (\sin\vartheta_j\cos\varphi_j, \sin\vartheta_j\sin\varphi_j, \cos\vartheta_j)\\ \zeta &= \sqrt{1-\boldsymbol{\xi}\cdot\boldsymbol{\xi}}\end{aligned} \tag{7}$$

where ζ is the z directed spectral wavenumber. As defined in (7), (ϑ_j, φ_j) are the conventional spherical angles with respect to the positive z axis (Fig. 2). Here and henceforth, upper or lower signs correspond to $j = 1$ or 2, respectively.

By applying (4) to the plane wave spectral representation in (6a) and inverting the order of integrations, one obtains for the time-dependent plane wave spectrum of the data $u_j(\mathbf{x}, t)$ the "slant stack transform" (SST)

$$\tilde{u}_j(\boldsymbol{\xi}, \tau) = \int d^2x u_j\big(\mathbf{x}, \tau + v_o^{-1}\boldsymbol{\xi}\cdot\mathbf{x}\big). \tag{8}$$

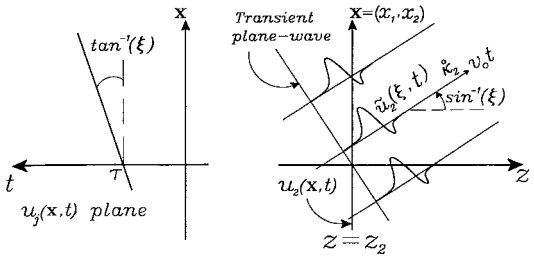

(a) (b)

Fig. 3. Transient plane wave spectrum. (a) Slant-stack transform (SST) of the field $u_j(\mathbf{x}, t)$. (b) Pulsed plane wave (PPW).

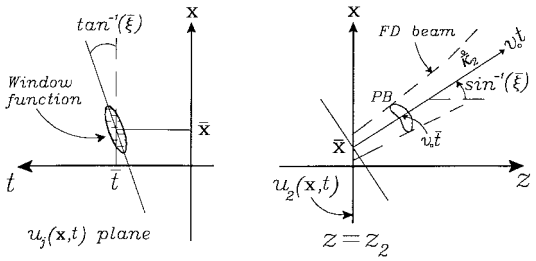

(a) (b)

Fig. 4. Local (pulsed-beam) spectrum. (a) Local SST of the field $u_j(\mathbf{x}, t)$. (b) Radiating pulsed beam (corresponding FD beam shown dashed).

The operation in (8) can be interpreted as a Radon transform in the 3-D $(\mathbf{x}, t)$ domain, consisting of projections of the data u_j onto the surfaces $t = \tau + v_o^{-1}\boldsymbol{\xi} \cdot \mathbf{x}$. Interpreted physically, for a given normalized wavenumber $\boldsymbol{\xi}$, the SST synthesizes the time-dependent spectra as a superposition of linearly time-delayed (slant-stacked) signals on the planes z_j, thereby extracting the TD plane wave information pertaining to the propagation direction $\boldsymbol{\xi}$ [Fig. 3(a)]. Note that the spectral range $|\boldsymbol{\xi}| < 1$ describes *propagating* transient plane waves, whereas the range $|\boldsymbol{\xi}| > 1$ describes *evanescent* transient plane waves that decay away from the initial plane. The inverse SST is obtained by inversion of the FD plane wave spectral representation in (6b)

$$u_j(\mathbf{x}, t) = \frac{-1}{(2\pi v_o)^2} \int d^2\xi \partial_t^2 \tilde{u}_j\big(\boldsymbol{\xi}, t - v_o^{-1}\boldsymbol{\xi} \cdot \mathbf{x}\big). \tag{9}$$

This result establishes the field at any space-time point $(\mathbf{x}, t)_j$ on the z_j planes as the sum of contributions from plane waves with time-delayed (slant-stacked) initial tilt angles specified by $\boldsymbol{\xi}$.

The plane wave spectral representation (9) of the data may readily be modified to describe the field away from the z_j planes. Although scattering plays no role here, we shall retain a notation that makes the formulation directly applicable to the scattering problem in Section IV. Since the scatterer is located *between* z_1 and z_2 (Fig. 1), scattering takes place along the negative z axis with respect to z_1 and along the positive z axis with respect to z_2. Thus, extension of the field data away from the "initial" planes z_1 and z_2 covers the regions $z < z_1$ and $z > z_2$, respectively. The resulting plane wave spectral integrals span both the propagating and evanescent spectral ranges $|\boldsymbol{\xi}| \lessgtr 1$, respectively. The contribution of the propagating spectrum by straightforward extension of (9) gives [4], [8]–[11]

$$u_j^{\text{prop}}(\mathbf{r}, t) = \frac{-1}{(2\pi v_o)^2} \int_{|\boldsymbol{\xi}|<1} d^2\xi \; \partial_t^2 \tilde{u}_j\big[\boldsymbol{\xi}, t - v_o^{-1}(\boldsymbol{\xi} \cdot \mathbf{x} \mp \zeta(z - z_j))\big] \quad z < z_1, \quad z > z_2. \tag{10}$$

This expression synthesizes the field at $(\mathbf{r}, t)$ in terms of an angular superposition of time-dependent plane waves [pulsed plane waves (PPW); see Fig. 3(b)]. The expression for the contribution u_j^{ev} of the evanescent spectrum is more complicated and may require the use of analytic signals as discussed after (5) (see, e.g., details in [9] and in [4, sec. 2.2.2]). This will not be considered here since the evanescent fields are not utilized in our imaging schemes.

2) Windowed Transform: For the desired *local* spectral analysis of the data, we generate the FD local plane wave spectrum via a windowed Fourier transform of the data in *configuration* space

$$\hat{U}_j(\mathbf{X}) = \int d^2x \hat{u}_j(\mathbf{x}) \hat{W}^*(\mathbf{x};\, \mathbf{X}) \tag{11}$$

where the asterisk denotes the complex conjugate and the kernel is given by $\hat{W}(\mathbf{x};\, \mathbf{X}) = \hat{w}(\mathbf{x} - \overline{\mathbf{x}})e^{ik\overline{\boldsymbol{\xi}}\cdot\mathbf{x}}$ with $\mathbf{X} = (\overline{\mathbf{x}}, \overline{\boldsymbol{\xi}})$. Here, $\hat{w}(\mathbf{x} - \overline{\mathbf{x}})$ is a spatial window function, centered at $\overline{\mathbf{x}} = (\overline{x}_1, \overline{x}_2)$ with linear phasing specified by $\overline{\boldsymbol{\xi}} = (\overline{\xi}_1, \overline{\xi}_2)$. The vector $\mathbf{X}$ incorporates the configuration-spectrum *phase-space coordinates* $(\overline{\mathbf{x}}, \overline{\boldsymbol{\xi}})$, whence $\hat{U}_j(\mathbf{X})$ is referred to as a *phase-space distribution* of the data $\hat{u}_j(\mathbf{x})$. The inverse phase-space transform is given formally by [12] and [13] and [4, eq. (27)]

$$\hat{u}_j(\mathbf{x}) = \left(\frac{k}{2\pi}\right)^2 \hat{N}^{-2} \int d^4X \hat{U}_j(\mathbf{X}) \hat{W}(\mathbf{x};\, \mathbf{X}) \tag{12}$$

where $\hat{N} = [\int d^2x |\hat{w}(\mathbf{x})|^2]^{1/2}$ is the $\mathcal{L}^2_{\mathbf{x}}$ norm of $\hat{w}$. The integral representation in (12) synthesizes the data as a phase-space superposition of all local spectral contributions $\overline{\boldsymbol{\xi}}$ from all points $\overline{\mathbf{x}}$. The transform (11) extracts from $\hat{u}_j$ the local spectrum around the $\overline{\boldsymbol{\xi}}$-directed propagation at the window center $\overline{\mathbf{x}}$. In typical scattering problems, the spectrum at a given $\overline{\mathbf{x}}$ is localized about a preferred spectral direction $\overline{\boldsymbol{\xi}}$ $(\overline{\mathbf{x}})$ that describes the direction of arrival of the scattered field at this point. Consequently, the local spectrum $\hat{U}_j(\mathbf{X})$ [and, thus, the inverse transform (12)] is localized *a priori* about the subdomain $(\overline{\mathbf{x}}, \overline{\boldsymbol{\xi}}) = (\overline{\mathbf{x}}, \overline{\boldsymbol{\xi}}(\overline{\mathbf{x}}))$ in the $\mathbf{X}$ domain (see synthetic examples in [4] and [13]; also see Fig. 4).

The time dependent *local* spectrum of the data is defined as the inverse Fourier transform (4) of $\hat{U}_j(\mathbf{X};\, \omega)e^{ik\overline{\boldsymbol{\xi}}\cdot\overline{\mathbf{x}}}$ (see interpretation of the linear phase after (15) and in [9])

$$U_j(\mathbf{Y}) = \frac{1}{2\pi} \int d\omega \hat{U}_j(\mathbf{X};\, \omega) e^{-i\omega(\overline{t} - v_o^{-1}\overline{\boldsymbol{\xi}}\cdot\overline{\mathbf{x}})} \tag{13}$$

where $\overline{t}$ denotes the phase-space time variable in the five-dimensional phase-space domain $\mathbf{Y} \equiv (\overline{\mathbf{x}}, \overline{\boldsymbol{\xi}}, \overline{t}) = (\mathbf{X}, \overline{t})$. To deduce $U_j(\mathbf{Y})$ directly from the TD data, we insert (11) into (13) and interchange the orders of integration to obtain (see

[9] and [4, eq. (36)]

$$U_j(\mathbf{Y}) = \int d^2x \int dt\, u_j(\mathbf{x}, t) W(\mathbf{x}, t;\ \mathbf{Y}) \qquad (14)$$

where the space–time dependent window function W is given by

$$W(\mathbf{x}, t;\ \mathbf{Y}) = w\big[\mathbf{x} - \overline{\mathbf{x}},\, t - \overline{t} - v_o^{-1}\overline{\boldsymbol{\xi}} \cdot (\mathbf{x} - \overline{\mathbf{x}})\big] \qquad (15)$$

and the time-dependent window $w(\mathbf{x}, t)$ is the TD analog of $\hat{w}(\mathbf{x})$ obtained via (4). The space-time and spectral dependence in the phase-space window W of (15) implies that the window is localized about $(\overline{\mathbf{x}}, \overline{t})$ with spectral tilt $\overline{\boldsymbol{\xi}}$ as schematized in Fig. 4(a). The operation in (14) can be referred to as a "*local slant-stack transform*" that extracts the local spectral information from the time-dependent data. Note that the linear phase introduced in (13) causes the TD local transform to be localized about $(\mathbf{x}, t) = (\overline{\mathbf{x}}, \overline{t})$.

To synthesize the data from the phase-space distribution (14) [i.e., to invert (14)], we apply (4) to (12) and follow essentially the same analytic steps as in (13)–(15), to obtain

$$u_j(\mathbf{x}, t) = -(2\pi v_o)^{-2} \int d^5Y U_j(\mathbf{Y}) W_N(\mathbf{x}, t;\ \mathbf{Y}) \qquad (16)$$

where $W_N(\mathbf{x}, t;\ \mathbf{Y}) \equiv N^\dagger(t) \overset{t}{\otimes} W(\mathbf{x}, t;\ \mathbf{Y})$ with $\overset{t}{\otimes}$ defined after (5) being a time-convolution and $N^\dagger(t) \equiv 1/2\pi \int d\omega (-i\omega)^2\ [\hat{N}(\omega)]^{-2} e^{-i\omega t}$ with $\hat{N}(\omega)$ defined after (12). Any formal convergence problems in $N^\dagger$ that may arise as $\omega \to \infty$ are avoided for practical finite-bandwidth signals with upper frequency limits.

The windowed integral representation in (16) synthesizes the space-time data as a phase-space superposition of *all* local spectral contributions $\overline{\boldsymbol{\xi}}$ from *all* points $\overline{\mathbf{x}}$. Recalling the discussion following (12), the windowed spectrum at a point $\overline{\mathbf{x}}$ is typically concentrated around a time $\overline{t}(\overline{\mathbf{x}})$ and wavenumber (or wave-tilt) $\overline{\boldsymbol{\xi}}(\overline{\mathbf{x}})$ that describe the arrival time and direction of the scattered field at that point. The inverse transform (16) at $(\mathbf{x}, t)$ is, therefore, localized *a priori* about the phase-space subdomain $\mathbf{Y}(\overline{\mathbf{x}}) = (\overline{\mathbf{x}}, \overline{\boldsymbol{\xi}}(\overline{\mathbf{x}}), \overline{t}(\overline{\mathbf{x}}))$.

3) Phase-Space Propagation: The phase-space superpositions in (12) can be used to track the FD field from the initial condition on the z_j planes forward and backward through the medium. For outward propagation in the $\mathbf{r}$-domain ($z \gtrless z_j$), each window kernel $\hat{W}(\mathbf{x};\ \mathbf{X})$ gives rise to a propagating beam field $\hat{B}_j(\mathbf{r};\ \mathbf{X})$ whose axis emerges from $\overline{\mathbf{x}}$ on the initial plane (z_j) in a direction determined by $\overline{\boldsymbol{\xi}}$ via (cf. 7)

$$\overset{\circ}{\overline{\boldsymbol{\kappa}}}_j = (\overline{\boldsymbol{\xi}}, \mp\overline{\zeta}), \quad \overline{\zeta} = \sqrt{1 - \overline{\boldsymbol{\xi}} \cdot \overline{\boldsymbol{\xi}}}. \qquad (17)$$

The resulting field representation is the same as (12) but with the window function $\hat{W}(\mathbf{x};\ \mathbf{X})$ replaced by the beam propagator $\hat{B}_j(\mathbf{r};\ \mathbf{X})$ (see Fig. 4(b); for detailed expressions see [4, eq. (28)] and [13]). Thus, the fields at $z \gtrless z_j$ are synthesized via a phase-space superposition of beams emerging from all points $\overline{\mathbf{x}}$ on the initial surfaces in all directions.

In the TD, each window kernel $W_N(\mathbf{x}, t;\ \mathbf{Y})$ in (16) gives rise to a propagating PB field $B_j(\mathbf{r}, t;\ \mathbf{Y})$ in the $(\mathbf{r}, t)$ domain, whose axis emerges from $\overline{\mathbf{x}}$ on the initial (x_j) plane in a direction determined by $\overline{\boldsymbol{\xi}}$ at the excitation time $\overline{t}$. The field representation is the same as in (16) but with the window function $W_N(\mathbf{x}, t;\ \mathbf{Y})$ replaced by the PB propagators $B_j(\mathbf{r}, t;\ \mathbf{Y})$ [4, eq. (44)], i.e., the field is expressed as a phase-space spectrum of PB's emerging from all points on the initial planes at all initial times $\overline{t}$ and in all directions $\overline{\boldsymbol{\xi}}$ with excitation amplitude given by the local spectrum $U_j(\mathbf{Y})$ that matches the PB to the phase-space space-time initial distribution. Explicit expressions for B_j may be found in [4, Eqs. (45), (46), and (69)], which are used in [2, eq. (6)] in connection with the forward and backward propagation of the measured data.

As discussed in connection with (16), the TD phase-space representation is localized *a priori* around the coordinates $(\overline{\mathbf{x}}, \overline{\boldsymbol{\xi}}(\overline{\mathbf{x}}), \overline{t}(\overline{\mathbf{x}}))$ since the local spectrum of the data $U_j(Y)$ is concentrated there. Further localization is effected by the PB propagators $B_j(\mathbf{r}, t;\ \mathbf{Y})$, which are concentrated around the trajectories in (17). This constrains the phase-space integration domain to the vicinity of the "observation constraint" $\mathbf{Y}(\mathbf{r}, t)$ whose $(\overline{\mathbf{x}}, \overline{\boldsymbol{\xi}}, \overline{t})$ coordinates are defined by

$$\frac{\mathbf{x} - \overline{\mathbf{x}}}{\mp(z - z_j)} = \frac{\overline{\boldsymbol{\xi}}}{\overline{\zeta}}, \quad \overline{t} = t - v_o^{-1}\sqrt{|\mathbf{x} - \overline{\mathbf{x}}|^2 + (z - z_j)^2}. \qquad (18)$$

IV. Spectral Analysis and Synthesis in a Weakly Perturbed Environment

Next we apply the spectral analysis tools described above to explore weak scattering by compact inhomogeneities which can be characterized by the Born approximation. The resulting Born-approximated data will be analyzed with a view toward establishing spectrum-object relations that lead in [2] to inversion of the scattered field data gathered on the z_j observation planes of Fig. 1.

A. The Born Approximation

The scattered field at z_j due to an inhomogeneity as in (2) with bounded support between the data planes (Fig. 1) can be expressed as a superposition of the fields radiated by induced volume sources whose strength is determined implicitly by an integral equation that defines the field in the medium [14]. For weak scattering scenarios, the induced source strengths at $\mathbf{r}'$ in the object domain are taken to be proportional to the incident field at $\mathbf{r}'$ in what constitutes the lowest order (Born) approximation. Following this route, the Born-approximated scattered time-harmonic field on z_j is given by

$$\hat{u}_j(\mathbf{r}) = \int d^3r' k^2 O(\mathbf{r}') \hat{u}^i(\mathbf{r}') \hat{G}(\mathbf{r};\ \mathbf{r}')|_{\mathbf{r} \in z_j \text{ planes}} \qquad (19)$$

with $\hat{u}^i(\mathbf{r}) = \hat{f}(\omega) e^{ikz}$ being the FD counterpart of the incident plane wave in (3) and $\hat{G}(\mathbf{r};\ \mathbf{r}') = e^{ik|\mathbf{r}-\mathbf{r}'|}/4\pi|\mathbf{r} - \mathbf{r}'|$ being the free-space Green's function. The conditions under which this approximation is valid are discussed in [15]. Likewise, the time-dependent Born approximation of the scattered field data is given by

$$u_j(\mathbf{x}, t) = -v_o^{-2}\partial_t^2 \int d^3r' \int dt' O(\mathbf{r}') u^i(\mathbf{r}', t') \cdot G(\mathbf{r}, t;\ \mathbf{r}', t'))|_{\mathbf{r} \in z_j \text{ planes}} \qquad (20)$$

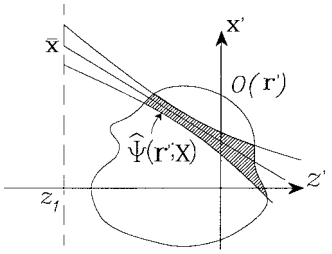

Fig. 5. FD local spectrum—object relation in (21). For specified $\mathbf{X}$, $\hat{U}_j(\mathbf{X})$ accounts only for contributions from $O(\mathbf{r}')$ sampled over the domain of influence of $\hat{\Psi}_j(\mathbf{r}';\ \mathbf{X})$.

where $G(\mathbf{r}, t;\ \mathbf{r}', t') = \delta(t - t' - v_o^{-1}|\mathbf{r} - \mathbf{r}'|)/4\pi|\mathbf{r} - \mathbf{r}'|$ and u^i is the incident pulsed plane wave in (3).

B. Phase-Space Scattering Propagators

Using (19) or (20) to express the scattered fields on the z_j-planes generated by the Born-approximated induced sources, we can now apply all of the phase-space manipulations in Section III pertaining to such fields. In particular, we shall be interested in the scattered field representations as established by the local spectral analysis in Section III-B2. Applying (11) to (19), we obtain after inverting the order of the $\mathbf{r}'$ and $\mathbf{x}$ integrations

$$\hat{U}_j(\mathbf{X}) = k^2 \hat{f}(\omega) \int d^3r' O(\mathbf{r}') e^{ikz'} \hat{\Psi}_j(\mathbf{r}';\ \mathbf{X}), \quad \mathbf{X} = (\overline{\mathbf{x}}, \overline{\boldsymbol{\xi}}) \tag{21}$$

where $\hat{\Psi}_j(\mathbf{r}';\ \mathbf{X})$ is the local spectrum of $\hat{G}$ sampled on the planes $z = z_j$, i.e.,

$$\hat{\Psi}_j(\mathbf{r}';\ \mathbf{X}) = \int d^2x \hat{W}^*(\mathbf{x};\ \mathbf{X}) \hat{G}(\mathbf{r};\ \mathbf{r}')|_{\mathbf{r} \in z_j \text{ planes}}. \tag{22}$$

In (21), the phase-space scattering propagators $\hat{\Psi}_j(\mathbf{r}';\ \mathbf{X})$ map the induced sources $k^2 \hat{f}(\omega) O(\mathbf{r}') e^{ikz'}$ from the object domain $\mathbf{r}'$ onto the local spectrum $\hat{U}_j(\mathbf{X})$.

If the window function $\hat{w}$ is "wide" on a wavelength scale, then for $|\overline{\boldsymbol{\xi}}| < 1$, the windowed phase-space objects $\hat{\Psi}_j$ behave like collimated beams in the $\mathbf{r}'$ domain whose axes reach points $\overline{\mathbf{x}}$ on the z_j planes along the directions $\overset{\circ}{\overline{\boldsymbol{\kappa}}}_j$ in (17). In view of (21), the local spectrum of the data $\hat{U}_j(\mathbf{X})$ accounts only for contributions from the object domain $O(\mathbf{r}')$ sampled by the domain of influence of $\hat{\Psi}_j$ in the vicinity of the beam axis corresponding to $\mathbf{X}$ (Fig. 5).

In the TD, Fourier inversion from the FD yields, by applying (13) to (21) and performing the ω integration first (or directly in the TD by applying (14) to (20), see also [3])

$$U_j(\mathbf{Y}) = -v_o^{-2} \int d^3r' O(\mathbf{r}') \int dt' f^{(2)}(t' - v_o^{-1} z') \Psi_j(\mathbf{r}', t';\ \mathbf{Y}) \tag{23}$$

where $f^{(n)}(t) \equiv \partial_t^n f(t)$, and the wave functions $\Psi_j(\mathbf{r}', t';\ \mathbf{Y})$ are the TD counterpart of $\hat{\Psi}_j(\mathbf{r}';\ \mathbf{X})$ of (22), i.e.,

$$\Psi_j(\mathbf{r}', t';\ \mathbf{Y}) = \frac{1}{2\pi} \int d\omega e^{-i\omega(\overline{t} - t' - v_o^{-1} \overline{\boldsymbol{\xi}} \cdot \overline{\mathbf{x}})} \hat{\Psi}_j(\mathbf{r}', \omega;\ \mathbf{X}). \tag{24}$$

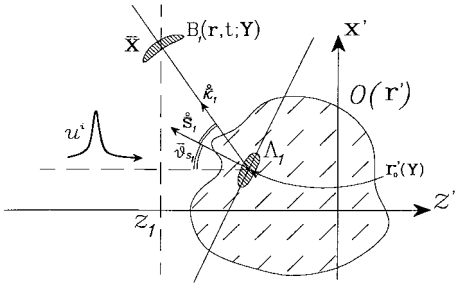

Fig. 6. TD local spectrum—object relation in (26). The figure shows the incident pulsed plane wave u^i and a scattered pulsed beam $B_1(\mathbf{r}, t;\ \mathbf{Y})$ in the $\overset{\circ}{\overline{\boldsymbol{\kappa}}}_1$ direction. This scattered PB is related via (26) to the local Radon transform of O sampled over the domain of influence of $\Lambda_j(\mathbf{r}';\ \mathbf{Y})$.

Inserting (22),

$$\Psi_j(\mathbf{r}', t';\ \mathbf{Y}) = \int d^2x \int dt W(\mathbf{x}, t;\ \mathbf{Y}) \cdot G(\mathbf{r}, t;\ \mathbf{r}', t')|_{\mathbf{r} \in z_j \text{ plane}} \tag{25}$$

which represents the local spectrum of G sampled on the z_j plane. [In the Appendix we also present a TD plane wave spectrum expression for Ψ_j, which will be used in (29) to determine the properties of the spatial sampling of the object implied by this window.] From (23), the phase-space scattering propagators Ψ_j map the field excited by the induced space-time sources $O(\mathbf{r}') f^{(2)}(t' - v_o^{-1} z')$ in the $(\mathbf{r}', t')$ domain onto the local spectrum of the data. The formulation in (23) can be recast so as to facilitate formal inversion of the object function. We rewrite (23) in the form

$$U_j(\mathbf{Y}) = f(\overline{t}) \overset{\overline{t}}{\otimes} \int d^3r' O(\mathbf{r}') \Lambda_j(\mathbf{r}';\ \mathbf{Y}) \tag{26}$$

where $\Lambda(\mathbf{r}';\ \mathbf{Y})$ is a sampling window in the object $(\mathbf{r}')$ domain given by

$$\Lambda(\mathbf{r}';\ \mathbf{Y}) = -v_o^{-2} \partial_{t'}^2 \Psi_j(\mathbf{r}', t';\ \mathbf{Y})\big|_{t' = v_o^{-1} z'} \tag{27}$$

Equation (26) is termed here the local (phase space) TD diffraction tomography relation: it represents the local spectrum of the time-dependent data in terms of local samples of $O(\mathbf{r})$ (Fig. 6). While in the FD relation (21), the kernel $\hat{\Psi}_j(\mathbf{r}', \omega;\ \mathbf{X})$ has the form of a beam that provides windowing of $O(\mathbf{r}')$ only transverse to the beam axis defined by $\mathbf{X}\Lambda_j$ in (26) provides windowing *also along* the beam axis as determined by the phase-space parameter $\mathbf{Y}$. In order to clarify the properties of this sampling, we explore the kernel Λ_j in detail in the next section.

C. Phase-Space Scattering Phenomenology

The localization effected by the PB propagators takes place along the beam axis, which is completely specified by the phase-space coordinates $\mathbf{Y}$ of the processing window on the data plane. In addition, the window orientation in the object domain is of interest. These aspects are best explored in the beam-centered coordinates $(z'_{b_j}, x'_{b_{1j}}, x'_{b_{2j}})$ in Fig. 7, which are oriented along the beam axis and along the two orthogonal directions perpendicular to the beam axis, respectively. The subscript j appended to the beam-centered coordinates

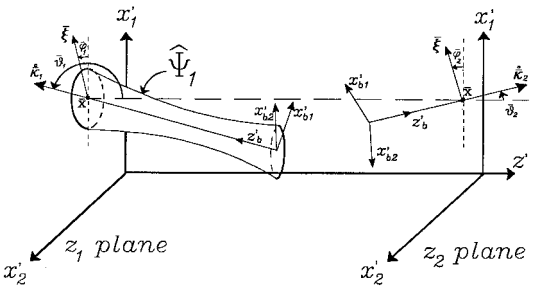

Fig. 7. Phase-space propagators. The phase-space propagators $\hat{\Psi}_j$ behave like collimated beams generated in the $\mathbf{r}'$ domain, whose axes reach points $\overline{\mathbf{x}}$ on the z_j planes, respectively, along the directions of the beam axis unit-vectors $\overset{\circ}{\overline{\boldsymbol{\kappa}}}_j$. The figure depicts the global fixed $(x_1,\, x_2,\, z)$ coordinate frame as well as the beam-centered coordinates $(z_{b_j}',\, x_{b1j}',\, x_{b_2j}')$ (referenced to the z_j planes, $j = 1,\, 2$), which extend along the beam axes and along the two orthogonal directions perpendicular to the beam axes, respectively.

identifies the relevant data plane z_j. For a given phase-space point $\mathbf{X}$, these coordinates will be defined explicitly in (46), but for the present discussion it is sufficient to note that $z_{b_j} < 0$ for points in the object domain ($z' \gtrless z_j$).

First, we determine the location $\mathbf{r}_o'(\mathbf{Y})$ of the center of Λ_j by noting that the PB data at time $\overline{t}$ on the z_j plane accounts for scattering at time $t' = \overline{t} + z_{b_j}'/v_o$ along the beam axis. Since the incident pulsed plane wave arrives at the scattering point at $t' = z'/v_o$, the center of Λ_j is determined by $z' = v_o\overline{t} + z_{b_j}'$. Using the geometrical relation $z' - z_j = z_{b_j}\cos\overline{\vartheta}_j$ we obtain $z_{b_j}' = -(v_o\overline{t} - z_j)/(1 - \cos\overline{\vartheta}_j)$. In the $(\mathbf{x},\, z)$ coordinates, the window center is given by

$$\mathbf{r}_o'(\mathbf{Y}) = (\overline{\mathbf{x}},\, z_j) - \overset{\circ}{\overline{\boldsymbol{\kappa}}}_j(v_o\overline{t} - z_j)/(1 - \cos\overline{\vartheta}_j) \tag{28}$$

where $(\overline{\mathbf{x}},\, z_j)$ is the intercept of the beam axis on the z_j plane and the unit vector $\overset{\circ}{\overline{\boldsymbol{\kappa}}}_j$ denotes the beam direction in (17) (see Fig. 6).

To determine the orientation of the sampling window Λ_j, we substitute the spectral representation of Ψ_j from (59) into (27) to find

$$\begin{aligned}\Lambda_j(\mathbf{r}';\, \mathbf{Y}) = \mathrm{Re}\frac{-1}{8\pi^2 v_o^3}\int d^2\xi \frac{1}{\zeta^*} \\ \overset{+}{\tilde{w}}{}^{(3)}\left[\boldsymbol{\xi} - \overline{\boldsymbol{\xi}},\, -\overline{t} + v_o^{-1}(-\boldsymbol{\xi}\cdot(\mathbf{x}' - \overline{\mathbf{x}}) \right. \\ \left. \pm \zeta^*(z' - z_j) + z')\right]\end{aligned} \tag{29}$$

where $\overset{+}{\tilde{w}}{}^{(3)}(\boldsymbol{\xi},\, \tau) = \partial_\tau^3 \overset{+}{\tilde{w}}$ and $\overset{+}{\tilde{w}}$ is the *analytic* TD plane wave spectrum of the analytic window $\overset{+}{w}(\mathbf{x},\, t)$ as calculated via (8) [as noted after (5), the analytic signal formulation is used here since Ψ_j involves both propagating and evanescent spectra]. The expression in (29) synthesizes Λ_j as a spectral superposition along planes weighted by the window function $\overset{+}{\tilde{w}}{}^{(3)}(\boldsymbol{\xi})$. Noting that $\overset{+}{\tilde{w}}$ peaks around the origin in the $(\boldsymbol{\xi},\, \tau)$ domain, the dominant spectral contribution in (29) is specified by the conditions

$$\boldsymbol{\xi} \simeq \overline{\boldsymbol{\xi}} \quad \text{and} \quad -\boldsymbol{\xi}\cdot(\mathbf{x}' - \overline{\mathbf{x}}) \pm \zeta(z' - z_j) + z' = v_o\overline{t}. \tag{30}$$

For specified $\mathbf{Y} = (\overline{\boldsymbol{\xi}},\, \overline{\mathbf{x}},\, \overline{t})$, (30) defines a (real) plane surface, which samples the object domain through its dependence on the primed coordinates. To understand the geometrical constraints implied by (30) we note from (17) that $\overset{\circ}{\overline{\boldsymbol{\kappa}}}_j - \overset{\circ}{\mathbf{z}} = (\overline{\boldsymbol{\xi}},\, \mp\overline{\zeta} - 1)$ and, thus, the plane-surface condition in (30) may be written as

$$-\left(\overset{\circ}{\overline{\boldsymbol{\kappa}}}_j - \overset{\circ}{\mathbf{z}}\right)\cdot[\mathbf{r}' - (\overline{\mathbf{x}},\, z_j)] = v_o\overline{t} - z_j \tag{31}$$

where, for convenience of interpretation, the $\mathbf{r}'$ coordinates are referred to the beam axis inception point $(\overline{\mathbf{x}},\, z_j)$. Next, we note that the vector $(\overset{\circ}{\overline{\boldsymbol{\kappa}}}_j - \overset{\circ}{\mathbf{z}})$ can be expressed as

$$\overset{\circ}{\overline{\boldsymbol{\kappa}}}_j - \overset{\circ}{\mathbf{z}} = 2\overset{\circ}{\overline{s}}_j\cos\overline{\vartheta}_{s_j} \tag{32}$$

where $\overset{\circ}{\overline{s}}_j$ is a unit vector and $\overline{\vartheta}_{s_j}$ is defined below. Equation (31) identifies $\overset{\circ}{\overline{s}}_j$ as the unit vector normal to the surface (30) and thus also to $\Lambda_j(\mathbf{r}';\, \mathbf{Y})$ of (27). It is convenient to express $\overset{\circ}{\overline{s}}_j$ in terms of the spherical coordinate angles $(\overline{\vartheta}_{s_j},\, \overline{\varphi}_{s_j})$ with respect to the *negative* z axis. One finds from (32) that

$$\overline{\vartheta}_{s_j} = \tfrac{1}{2}(\pi - \overline{\vartheta}_j) \quad \overline{\varphi}_{s_j} = \overline{\varphi}_j \tag{33}$$

where $(\overline{\vartheta}_j,\, \overline{\varphi}_j)$ are the angles of $\overset{\circ}{\overline{\boldsymbol{\kappa}}}_j$ with respect to the *positive* z axis [see (7) and (17)]. Thus, it follow from (33) that the sampling window is oriented so that its normal $\overset{\circ}{\overline{s}}_j$ bisects the angle between the direction of incidence (the negative z axis) and the spectral scattering direction $\overset{\circ}{\overline{\boldsymbol{\kappa}}}_j$ (see Fig. 6).

The above results imply that the interaction of the z-directed pulsed plane wave with the object domain, when parameterized in terms of scattered PB propagators, occurs as if each scattered PB were *specularly reflected* from the local medium inhomogeneities (Fig. 6). Each PB senses the medium as if it were locally a plane stratified medium along the bisectional $\overset{\circ}{\overline{s}}_j$ axis with the effective variations of the medium along this axis being extracted from $O(\mathbf{r})$ via the sampling operation in (26). This interpretation is a localized version of the "pseudo plane wave reflection law" discussed in connection with the transient plane wave analysis in [1].

The implications of the above will be illustrated by considering in detail two special window functions: A plane wave window (i.e., a nonwindowed transform) and a Gaussian δ window.

D. Special Case I: Plane Wave Window

1) Sampling Kernels and Scattered Field Spectra: For this special case, in the FD, $\hat{w}(\mathbf{x}) = 1$ and (11) reduces to the nonwindowed Fourier transform (6a) [i.e.,$\hat{\tilde{U}}_j(\overline{\mathbf{x}},\, \overline{\boldsymbol{\xi}}) \to \hat{u}_j(\overline{\boldsymbol{\xi}})$]. The results in this case are reduced to the conventional FD diffraction tomography relation [16], or the TD diffraction tomography in [1]. We shall summarize here only the TD results since they give important insight to the windowed results in Section IV-E.

In the TD, we have the impulsive plane wave window $w(\mathbf{x},\, t) = \delta(t)$. Thus, from (14), the local spectrum reduces to the SST in (8) $U_j(\mathbf{Y}) \to \tilde{u}_j(\overline{\boldsymbol{\xi}},\, \overline{t} - \overline{\boldsymbol{\xi}}\cdot\overline{\mathbf{x}})$; from (25), Ψ_j are PPW in the $\overset{\circ}{\overline{\boldsymbol{\kappa}}}_j$ direction and from (27) the sampling window

is found to be

$$\Lambda_j^{\mathrm{PW}}(\mathbf{r}';\ \mathbf{Y}) = \frac{-1}{2v_o\overline{\zeta}}\,\delta^{(1)}\left[\overline{t} - v_o^{-1}\left(-\overline{\boldsymbol{\xi}}(\mathbf{x}'-\overline{\mathbf{x}}) \pm \overline{\zeta}(z'-z_j)+z'\right)\right] \tag{34}$$

which defines the plane surface (Fig. 6) discussed in (30)–(33). Using (34), relation (26) reduces to

$$\tilde{u}_j(\overline{\boldsymbol{\xi}},\overline{t}) = f'(\overline{t}) \overset{\overline{t}}{\otimes} \frac{-1}{2\zeta v_o}\int d^3r'\ O(\mathbf{r}') \cdot \delta\Big(\overline{t} + v_o^{-1}[(\overset{\circ}{\overline{\boldsymbol{\kappa}}}_j - \overset{\circ}{\mathbf{z}})\cdot\mathbf{r}' \pm \overline{\zeta} z_j]\Big). \tag{35}$$

This result expresses the relation between the time-dependent plane wave spectrum of the data and the Radon transform of $O(\mathbf{r}')$ along the direction $\overset{\circ}{\overline{s}}_j$ that bisects the angle between the direction of incidence $\overset{\circ}{\boldsymbol{\kappa}}^i = \overset{\circ}{\mathbf{z}}$ and the spectral direction $\overset{\circ}{\overline{\boldsymbol{\kappa}}}_j$. In [1], this relation has been identified and interpreted as *TD diffraction tomography.*

2) Scattering Phenomenology: The form of the plane wave sampling kernel in (34) permits an incisive physical interpretation of the scattering mechanism. The results and their implications for plane wave diffraction tomography have been discussed previously [1]. Here, relevant portions will be summarized briefly in order to provide the background for the new pulsed-beam probing in Section IV-E.

Summarizing from [1], we introduce phenomenology-matched coordinates. Noting from (35) that the relevant temporal coordinate is $v_o\overline{t} = -(\overset{\circ}{\overline{\boldsymbol{\kappa}}}_j - \overset{\circ}{\mathbf{z}})\cdot\mathbf{r}' \mp \overline{\zeta} z_j$ and recalling (31) and (32), this condition defines a plane in the $\mathbf{r}'$ domain, perpendicular to the $\overset{\circ}{\overline{s}}_j$ axis whose distance from the origin $\mathbf{r}' = 0$ is given by

$$p_j = -\left(v_o\overline{t} + z_j\cos 2\overline{\vartheta}_{s_j}\right)/2\cos\overline{\vartheta}_{s_j}. \tag{36}$$

This condition defines a "pseudoreflection plane" that converts the incident pulsed plane wave $f(t-z/v_o)$ into a pulsed plane wave in the $\overset{\circ}{\overline{\boldsymbol{\kappa}}}_j$ direction arriving at the center $(\mathbf{x}=0)$ of the z_j plane at time $\overline{t}$. Thus, the spectral time-dependent plane wave in the $\overset{\circ}{\overline{\boldsymbol{\kappa}}}_j$ direction is generated by a pseudoplane-stratified medium whose axis is along the $\overset{\circ}{\overline{s}}_j$ direction, the spectral arrival time $\overline{t}$ being directly related to the location p_j of the reflecting plane along the $\overset{\circ}{\overline{s}}_j$ axis. Furthermore, since (35) can be recast as a Radon transform of $O(\mathbf{r})$ along the $\overset{\circ}{\overline{s}}_j$ axis, it follows that the pseudoplane stratified medium along $\overset{\circ}{\overline{s}}_j$ is characterized by the Radon transform of $O(\mathbf{r})$ along that axis. Further details concerning this interpretation can be found in [1]. A related result has been derived asymptotically in [17].

E. Special Case II: Gaussian δ Window

1) Window Profiles: It is advantageous to use Gaussian windows since they yield analytically trackable beam-type propagators. In the FD, we use a Gaussian window whose spatial and spectral distributions are

$$\begin{aligned}\hat{w}(\mathbf{x}) &= -\omega^2\alpha e^{-(1/2)k\beta^{-1}|\mathbf{x}|^2}e^{-\omega T/2},\\ \hat{\hat{w}}(\boldsymbol{\xi}) &= -\omega^2\alpha(2\pi\beta/k)e^{-(1/2)k\beta|\boldsymbol{\xi}|^2}e^{-\omega T/2}\end{aligned} \tag{37}$$

where the parameter $\beta = \beta_r + i\beta_i$, with $\beta_r > 0$ for $\omega > 0$, and with $\beta|_{\omega<0} = -\beta^*|_{\omega>0}$. Anticipating extension to the TD, (37) has been constructed so that the frequency $k = \omega/v_o$ appears explicitly in the exponent while β is *frequency independent* (except for the symmetry condition mentioned above). These features will be used later on to construct collimated TD wave objects. The role of the complex parameter α will be discussed in the inversion procedure in [2, eq. (42)]. The window in (37) also includes the factor $\omega^2\exp(-\omega T/2)$ whose role is to generate a well behaved window in the space-time domain [see (38)] that also satisfies $w(\mathbf{x},t)\in\mathcal{L}^1(\mathbf{x},t)$ as required for numerical implementation [4, sec. 4-2]. These additional parameters have not been included in the two-dimensional (2-D) phase-space analysis in [9] and [13]. The present theory also involves nontrivial extensions of the 2-D theory because of the skewing and consequent distortion of the beam propagators in the 3-D case.

Because of the constraint $\beta|_{\omega<0} = -\beta^*|_{\omega>0}$, it is convenient to transform (37) into the TD via the analytic signal transform in (5), giving the "Gaussian δ" window

$$w(\mathbf{x},t) = \mathrm{Re}\overset{+}{w}(\mathbf{x},t) = \mathrm{Re}\left(\alpha\overset{+}{\delta}{}^{(2)}\left[t - \frac{i}{2}T - \frac{i}{2}|\mathbf{x}|^2/v_o\beta\right]\right) \tag{38}$$

where $\overset{+}{\delta}$ is the analytic delta function

$$\overset{+}{\delta}(t) = \begin{cases}(\pi i t)^{-1}, & \text{Im t} \le 0\\ \delta(t) + \mathcal{P}(\pi i t)^{-1}, & \text{Im t} = 0\end{cases} \tag{39}$$

and $\overset{+}{\delta}{}^{(2)}(t) = 2/\pi i t^3$. This window is localized around $(\mathbf{x},t) = (0,0)$. Recalling that $\beta_r > 0$, the argument of the $\overset{+}{\delta}$ function in (38) has a negative imaginary part that increases quadratically with $|\mathbf{x}|$, thus generating a smooth Lorentzian window which is strongest for $|\mathbf{x}| = 0$ and weakens as $|\mathbf{x}|$ increases. To obtain sufficient resolution, the parameter $T > 0$ is chosen to satisfy

$$T \ll \omega_{\max}^{-1} \tag{40}$$

with $\omega_{\max}$ denoting the upper frequency in the incident signal.

To clarify the properties of the window in (38) we separate the argument of the $\overset{+}{\delta}$ function into real and imaginary parts and rewrite it in a standard form as

$$w(\mathbf{x},t) = \mathrm{Re}\left(\alpha\overset{+}{\delta}{}^{(2)}\left[t - t_p - \frac{i}{2}T_p\right]\right) \tag{41}$$

where

$$t_p(\mathbf{x}) = \frac{1}{2}\frac{\beta_i}{v|\beta|^2}|\mathbf{x}|^2, \qquad T_p(\mathbf{x}) = T + \frac{\beta_r}{v|\beta|^2}|\mathbf{x}|^2. \tag{42}$$

The interpretation of (41) is not compromised by ignoring the time derivative and assuming $\alpha = 1$ so that $w(\mathbf{x},t) = \pi^{-1}(T_p/2)/[(t-t_p)^2 + (T_p/2)^2]$. For given $\mathbf{x}$, the expression peaks at $t = t_p(\mathbf{x})$ and its pulse length and peak value are given, respectively, by $T_p(\mathbf{x})$ and $2/\pi T_p(\mathbf{x})$. Thus, as $|\mathbf{x}|$ increases, T_p increases and w decays. The transverse half-amplitude diameter D of the window is, therefore, obtained by solving $T_p(\mathbf{x}) = 2T_p(0)$, giving

$$D = 2\sqrt{T|\beta|^2 v_o/\beta_r}. \tag{43}$$

Further properties of this window, in particular those pertaining to numerical implementation for analysis of space–time data, have been explored in [4, sec. 4.2].

2) Phase-Space Scattering Propagators: If the window is "large" on a wavelength scale, the FD kernels $\hat{\Psi}_j(\mathbf{r}';\ \mathbf{X})$ in (22) yield collimated beam fields in the $\mathbf{r}'$ domain. Via asymptotic evaluation and paraxial approximation, one obtains

$$\hat{\Psi}_j(\mathbf{r}';\ \mathbf{X}) \sim \frac{-i\omega v_o \alpha^*}{2\overline{\zeta}} \sqrt{\frac{\det \mathbf{Q}_j(z'_{b_j})}{\det\ \mathbf{Q}_j(0)}} \cdot e^{-\omega T/2} e^{ik\,(\overline{\boldsymbol{\xi}}\cdot\overline{\mathbf{x}} - z'_{b_j} + (1/2)\mathbf{x}'_{b_j}\cdot\mathbf{Q}_j(z'_{b_j})\cdot\mathbf{x}'_{b_j})} \tag{44}$$

where

$$\mathbf{Q}_j(z'_{b_j}) \simeq \begin{bmatrix} (-z'_{b_j} - i\beta^*\overline{\zeta}^2)^{-1} & 0 \\ 0 & (-z'_{b_j} - i\beta^*)^{-1} \end{bmatrix}. \tag{45}$$

The derivation of this expression is similar to that presented in the Appendix of [4] in connection with the beam propagators $\hat{B}$. In (44) we utilize the beam coordinates $(x'_{b_{1j}}, x'_{b_{2j}}, z'_{b_j})$ defined, for a given phase-space point $\mathbf{X}$, by the transformation

$$\begin{bmatrix} x'_{b_{1j}} \\ x'_{b_{2j}} \\ z'_{b_j} \end{bmatrix} = \begin{bmatrix} \mp\cos\overline{\vartheta}_j\cos\overline{\varphi}_j & \mp\cos\overline{\vartheta}_j\sin\overline{\varphi}_j & \pm\sin\overline{\vartheta}_j \\ \pm\sin\overline{\varphi}_j & \mp\cos\overline{\varphi}_j & 0 \\ \sin\overline{\vartheta}_j\cos\overline{\varphi}_j, & \sin\overline{\vartheta}_j\sin\overline{\varphi}_j & \cos\overline{\vartheta}_j \end{bmatrix} \cdot \begin{bmatrix} x'_1 - \overline{x}_1 \\ x'_2 - \overline{x}_2 \\ z' - z_j \end{bmatrix} \tag{46}$$

where $(\overline{\vartheta}_j, \overline{\varphi}_j)$ are the spherical angles associated with $\overset{\circ}{\overline{\boldsymbol{\kappa}}}_j$ of (17) and upper and lower signs correspond to $j = 1, 2$, respectively, (see Fig. 7). Thus, the z'_{b_j} axes coincide with the beam axes in the positive (outward) $\overset{\circ}{\overline{\boldsymbol{\kappa}}}_j$ direction; the transverse coordinates $\mathbf{x}'_{b_j} = (x'_{b_{1j}}, x'_{b_{2j}})$ are rotated such that $x'_{b_{2j}}$ is parallel to the z plane while $x'_{b_{1j}}$ lies in the plane $(\overline{\boldsymbol{\xi}}, \overset{\circ}{\overline{\boldsymbol{\kappa}}}_j)$ (see Fig. 7) with its positive direction defined so that $\overline{\boldsymbol{\xi}} \cdot \overset{\circ}{\mathbf{x}}'_{b_{1j}} > 0$. Furthermore, the systems $(\mathbf{x}'_{b_j}, z'_{b_j})$ are defined to be right handed. Accordingly, the linear phase $\overline{\boldsymbol{\xi}} \cdot \mathbf{x}'$ implied by the window function in the $z = z_j$ planes is operative in the $x'_{b_{1j}}$ direction *but not* in the $x'_{b_{2j}}$ direction. Consequently, $\overline{\boldsymbol{\xi}}$ affects only the Q_{11} term in (45), but not the Q_{22} term, thereby describing *astigmatic* beams.

The TD phase-space scattering propagators $\Psi_j(\mathbf{r}', t', \mathbf{Y})$ due to the window in (38) can be found by evaluating the TD spatial or spectral integrals in (25) and (59), respectively, or by transforming the FD expression via (24). Near the beam axis we obtain closed-form expressions by transforming (44) via (24), giving

$$\Psi_j(\mathbf{r}', t';\ \mathbf{Y}) \sim \mathrm{Re}\frac{v_o\alpha^*}{2\overline{\zeta}} \sqrt{\frac{\det \mathbf{Q}_j(z'_{b_j})}{\det \mathbf{Q}_j(0)}} \overset{+}{\delta}{}^{(1)}\left[\overline{t} - t' - \frac{1}{2}T - v_o^{-1}\left(-z'_{b_j} + \frac{1}{2}\mathbf{x}'_{b_j}\cdot\mathbf{Q}_j\cdot\mathbf{x}'_{b_j}\right)\right]. \tag{47}$$

This expression describes a pulsed beam (space–time wavepacket) whose center follows the trajectory $t' - z'_{b_j}/v_o = \overline{t}$; thus contributions to the phase-space data at $\overline{t}$ arrive from points in the $(\mathbf{r}', t')$ domain near the PB center described by this trajectory. As in (41), the spatial confinement transverse to the beam axis is described by the quadratic form $-1/2v_o^{-1}\mathbf{x}'_{b_j}\cdot\mathbf{Q}_j\cdot\mathbf{x}'_{b_j}$, which (since $\beta_r > 0$) has a negative imaginary part that increases quadratically as the distance from the axis increases. To clarify the wavepacket structure one should separate the argument of the $\overset{+}{\delta}$ function into real and imaginary parts and follow the procedure detailed in (41). We therefore rewrite the elements of $\mathbf{Q}_j$ in the form

$$(-z'_{b_j} + Z_l - iF_l)^{-1} \equiv 1/R_l + i/I_l \tag{48}$$

where $l = 1$ or 2 correspond to $x_{b_{1j}}$ and $x_{b_{2j}}$, respectively, and Z_l and F_l are given by

$$Z_1 = -\beta_i\overline{\zeta}^2, \quad F_1 = \beta_r\overline{\zeta}^2, \quad Z_2 = -\beta_i, \quad F_2 = \beta_r. \tag{49}$$

Thus, R_l and I_l are given by

$$R_l(z'_{b_j}) = -(z'_{b_j} - Z_l) - F_l^2/(z'_{b_j} - Z_l) \tag{50}$$

$$I_l(z'_{b_j}) = F_l + (z'_{b_j} - Z_l)^2/F_l. \tag{51}$$

Equation (47) for the PB field may therefore be written in the form

$$\Psi_j(\mathbf{r}', t';\ \mathbf{Y}) = \mathrm{Re}\frac{v_o\alpha^*}{2\overline{\zeta}} \sqrt{\frac{(Z_1 - iF_1)(Z_2 - iF_2)}{(-z'_{b_j} + Z_1 - iF_1)(-z'_{b_j} + Z_2 - iF_2)}} \cdot \overset{+}{\delta}{}^{(1)}\left[\overline{t} - t' + t_p(\mathbf{r}') - \frac{i}{2}T_p(\mathbf{r}')\right] \tag{52}$$

where the real and imaginary parts of the argument of $\overset{+}{\delta}{}^{(1)}$ are

$$t_p(\mathbf{r}') = v_o^{-1}\left(z'_{b_j} - x'^2_{b_{1j}}/2R_1 - x'^2_{b_{2j}}/2R_2\right) \tag{53}$$

$$T_p(\mathbf{r}') = T + v_o^{-1}\left(x'^2_{b_{1j}}/I_1 + x'^2_{b_{2j}}/I_2\right). \tag{54}$$

Equation (52) with (53) and (54) is readily identified as an astigmatic PB along the z'_{b_j} axis whose major transverse axes are $(x'_{b_{1j}}, x'_{b_{2j}})$, with R_l representing the wavefront radii of curvature in the $x'_{b_{lj}}$ directions. Moreover, $t_p(\mathbf{r}')$ is the paraxial propagation delay while $T_p(\mathbf{r}')$ is the temporal half-amplitude length of the $\overset{+}{\delta}$ pulse, which is inversely proportional to the pulse amplitude. Thus, the field is strongest on the beam axis where $T_p(\mathbf{r}')$ is minimal and it decays as T_p increases away from the beam axis. Analogous to (43), the half-amplitude beam diameter in the $x'_{b_{lj}}$ directions is found by solving $T_p(x_{b_{lj}}) = 2T_p(0)$, giving

$$D_{l_j}\left(z'_{b_j}\right) = 2\sqrt{v_o T I_l\left(z'_{b_j}\right)}. \tag{55}$$

Thus, the collimation lengths in the $(x'_{b_{lj}}, z')$ cross-sectional planes are F_l and the waists are located at $z'_{b_j} = Z_l$ with widths $2\sqrt{v_o T F_l}$. From (54) with (51), one notes that in the collimation (Fresnel) zone $|z'_{b_j} - Z_l| < F_l$, the PB is essentially unchanged, whereas outside this zone the beam opens up along the far-field diffraction angles $\Theta_l = 2\sqrt{v_o T/F_l}$.

As mentioned earlier, the propagator (52) belongs to the general class of PB fields in [5] and [6], termed isodiffracting [7]. Thus, all frequency components of the PB's in (52) are Gaussian beams with the *same* collimation distance and radii of curvature. Since these beams are generated by the Gaussian window in (37) with frequency independent β, the window width is proportional to $\omega^{-1/2}$.

3) The Phase-Space Sampling Kernels: Inserting (47) into (27), we obtain the sampling window in the $\mathbf{r}'$ (object) domain

$$\Lambda_j(\mathbf{r}';\ \mathbf{Y}) \sim \mathrm{Re}\frac{-\alpha^*}{2v_o\overline{\zeta}}\sqrt{\frac{\det \mathbf{Q}_j(z'_{b_j})}{\det \mathbf{Q}_j(0)}} \cdot \overset{+}{\delta}{}^{(3)}\left[\overline{t} - \frac{i}{2}T - v_o^{-1}\left(z' - z'_{b_j} + \frac{1}{2}\,\mathbf{x}'_{b_j}\cdot\mathbf{Q}_j\cdot\mathbf{x}'_{b_j}\right)\right]. \tag{56}$$

In order to show that this window satisfies the general properties discussed in (31) we denote $\psi \equiv z' - z'_{b_j} + \frac{1}{2}\mathbf{x}'_{b_j}\cdot\mathbf{Q}_j\cdot\mathbf{x}'_{b_j}$. The window peaks at points $\mathbf{r}'$ satisfying $\psi = 0$, i.e., at $\mathbf{r}'_o(\mathbf{Y})$ in (28) on the PB axis. Off the PB axis, the window peaks at points $\mathbf{r}'$ satisfying $\mathrm{Re}\psi(\mathbf{r}') = v_o\overline{t}$, so that the normal to the window at $\mathbf{r}'_o$ can be found via $\overset{\circ}{\overline{s}}_j = (\nabla\ \mathrm{Re}\ \psi/|\nabla\ \mathrm{Re}\ \psi|)|_{\mathbf{r}'_o}$. Calculating this expression we find that $\overset{\circ}{\overline{s}}_j$ satisfies the properties discussed in connection with (33) and Fig. 6.

V. Conclusions

In this paper, which is the first part of a two-part sequence, we have extended the previously developed PPW-based time-domain diffraction tomography for forward Born-type scattering in [1] to a more localized PB-parameterized version, which, in contrast to the global planar PPW wavefronts, confines interrogation of the scattering domain to scattering cells centered along the beam axis. Operating in the configuration-spectrum phase space accessed by windowed transforms, we have developed the PB-based mathematical methodology for forward scattering and have endeavored to explain the results in terms of physically meaningful wave phenomena, thereby laying the foundation for the inversion procedure in [2]. To highlight the differences between the PPW- and PB-based algorithms, the scattered field alone has been decomposed into PB's while leaving the PPW incident wave intact. This hybrid global–local setting has interesting phenomenological implications; although the PPW excitation of the scattering medium gives rise to induced point radiators distributed along the entire instantaneous wavefront, the PB-processed scattered field arises solely from the relevant local scattering cell, as observed along the beam axis direction. The latter feature suggests that "constrained ray" (i.e., beam) trajectories characterize the scattering in this scenario, thereby leading to a reinterpretation of the PPW one-dimensional "pseudoreflection rule" in [2] in terms of beam-constrained Fermat paths of least travel time. This interpretation will turn out to be *the* logical outcome when the problem is "ultimately localized" via PB-processed exciting *and* scattered fields, as discussed briefly in [2, sec. VI].

Appendix
Time-Domain Spectral Representation of Ψ_j

We start with the well know spectral expression of the FD Green's function

$$\hat{G}(\mathbf{r};\mathbf{r}') = \left(\frac{k}{2\pi}\right)^2 \int d^2\xi \frac{1}{-2ik\zeta}\, e^{ik(\xi\cdot(\mathbf{x}-\mathbf{x}')+\zeta|z-z'|)}. \tag{57}$$

Substituting in (22) and inverting the order of integrations yields the plane wave representation

$$\hat{\Psi}_j(\mathbf{r}';\ \mathbf{X}) = \frac{i\omega}{8\pi^2 v_o}\int d^2\xi\zeta^{-1}\left[\hat{\overset{+}{W}}(\boldsymbol{\xi};\ \mathbf{X})\right]^* \cdot e^{ik(-\xi\cdot\mathbf{x}'+\zeta|z_j-z'|)} \tag{58}$$

where $\hat{\overset{+}{W}}(\boldsymbol{\xi};\ \mathbf{X}) = \hat{\overset{+}{w}}(\boldsymbol{\xi}-\overline{\boldsymbol{\xi}})e^{-ik(\xi-\overline{\xi})\cdot\overline{\mathbf{x}}}$ with $\hat{\overset{+}{W}}$ and $\hat{\overset{+}{w}}$ being the spectral functions in (6a) corresponding to $\hat{W}$ and $\hat{w}$, respectively. The TD counterpart of (58) is obtained via (24). It is convenient to use the analytic signal formulation as effected by the one-sided Fourier inversion [see (5)]. Thus, applying the one-sided counterpart of (24) to (58) and inverting the order of integrations, we obtain

$$\Psi_j(\mathbf{r}',t';\ \mathbf{Y}) = \mathrm{Re}\frac{1}{8\pi^2 v_o}\int d^2\xi\frac{1}{\zeta^*} \partial_{t'}\overset{+}{W}\left[\boldsymbol{\xi},\ t' + v_o^{-1}(-\boldsymbol{\xi}\cdot\mathbf{x}' \pm \zeta^*(z'-z_j))\ \mathbf{Y}\right] \tag{59}$$

where $\overset{+}{W}(\boldsymbol{\xi},\tau;\ \mathbf{Y}) = \overset{+}{w}(\boldsymbol{\xi}-\overline{\boldsymbol{\xi}},\ \tau-\overline{t}+v_o^{-1}\boldsymbol{\xi}\cdot\overline{\mathbf{x}})$ is the analytic transient plane-wave spectrum of $\overset{+}{W}$ [cf. (15)].

References

[1] T. Melamed, Y. Ehrlich, and E. Heyman, "Short-pulse inversion of inhomogeneous media: A time-domain diffraction tomography," *Inverse Problems*, vol. 12, pp. 977–993, 1996.

[2] T. Melamed, E. Heyman, and L. B. Felsen, "Local spectral analysis of short-pulse excited scattering from weakly inhomogeneous media—Part II: Inverse scattering," *IEEE Trans. Antennas Propagat.*, this issue, pp. 1218–1227.

[3] T. Melamed and E. Heyman, "Spectral analysis of time-domain diffraction tomography," *Radio Sci.*, vol. 32, pp. 593–604, 1997.

[4] T. Melamed, "Phase-space beam summation: A local spectrum analysis for time-dependent radiation," *J. Electromagn. Waves Appl.*, vol. 11, pp. 739–773, 1997.

[5] E. Heyman and L. B. Felsen, "Complex source pulsed beam fields," *J. Opt. Soc. Amer.* vol. 6, pt. A, 806–817, 1989.

[6] E. Heyman, "Pulsed beam propagation in an inhomogeneous medium," *IEEE Trans. Antennas Propagat.*, vol. 42, pp. 311–319, 1994.

[7] E. Heyman and T. Melamed, "Certain considerations in aperture synthesis of ultrawideband/short-pulse radiation," *IEEE Trans. Antennas Propagat.*, vol. 42, pp. 518–525, 1994.

[8] E. Heyman and L. B. Felsen, "Weakly dispersive spectral theory of transients (STT): Part I—Formulation and interpretation; Part II—Evaluation of the spectral integral; Part III—Applications," *IEEE Trans. Antennas Propagat.*, vol. AP-35, pp. 80–86; pp. 574–580; pp. 1258–1266, 1987.

[9] B. Z. Steinberg, E. Heyman, and L. B. Felsen, "Phase space beam summation for time dependent radiation from large apertures: Continuous parametrization," *J. Opt. Soc. Amer. A*, vol. 8, no. 943–958, 1991.

[10] T. B. Hansen and A. D. Yaghjian, "Planar near-field scanning in the time-domain—Part I: Fomulation," *IEEE Trans. Antennas Propagat.*, vol. 42, pp. 1280–1291, 1994.

[11] T. B. Hansen and A. D. Yaghjian, "Planar near-field scanning in the time-domain: Part II—Sampling theorem and computation schemes," *IEEE Trans. Antennas Propagat.*, vol. 42, no. 1292–1300, 1994.

[12] M. J. Bastiaans, "Signal descriptions by means of a local frequency spectrum," in *Proc. SPIE: Transformat. Opt. Signal Processing*, vol. 373, pp. 49–62, 1981.
[13] B. Z. Steinberg, E. Heyman, and L. B. Felsen, "Phase space beam summation for time-harmonic radiation from large apertures," *J. Opt. Soc. Amer.*, vol. 8, pt. A, no. 41–59, 1991.
[14] J. R. Taylor, *Scattering Theory*. New York: Wiley, 1972.
[15] J. B. Keller, "Accuracy and validity of the Born and Rytov approximations," *J. Opt. Soc. Amer.*, vol. 59, pp. 1003–1004, 1969.
[16] A. J. Devaney, "Diffraction tomography," in *Inverse Methods in Electromagnetic Imaging—Part II*, W. M. Boerner, Ed. Dodrecht, Holland: Reidel, 1985.
[17] D. Miller, M. Orstaglio, and G. Beylkin, "A new slant on seismic imaging: Migration and integral geometry," *Geophys.*, vol. 52, no. 943–964, 1987.

Timor Melamed was born in Tel-Aviv, Israel, in January 1964. He received the B.Sc. degree (*magma cum laude*) in electrical engineering and the Ph.D. degree, both from Tel-Aviv University, in 1989 and 1997, respectively.

From 1989 to 1990, he worked on microprocessor design at National Semiconductor, Tel Aviv, Israel. From 1996 to 1998 he held a postdoctoral position at the Department of Aerospace and Mechanical Engineering, Boston University, MA. He is currently with Odin Technologies, Yokne'am, Israel. His main fields of interest are analytic techniques in wave theory, transient wave phenomena, and inverse scattering.

Ehud Heyman (S'80–M'82–SM'88), for a photograph and biography, see p. 528 of the May 1995 issue of this TRANSACTIONS.

Leopold B. Felsen (S'47–A'53–M'54–SM'55–F'62–LF'90), photograph and biography not available at the time of publication.